SCIENTIFIC REP⚙RTS

OPEN

Uniting Superhydrophobic, Superoleophobic and Lubricant Infused Slippery Behavior on Copper Oxide Nano-structured Substrates

Sanjeev Kumar Ujjain, Pritam Kumar Roy, Sumana Kumar, Subhash Singha & Krishnacharya Khare

Alloys, specifically steel, are considered as the workhorse of our society and are inimitable engineering materials in the field of infrastructure, industry and possesses significant applications in our daily life. However, creating a robust synthetic metallic surface that repels various liquids has remained extremely challenging. The wettability of a solid surface is known to be governed by its geometric nano-/micro structure and the chemical composition. Here, we are demonstrating a facile and economical way to generate copper oxide micro-nano structures with spherical (0D), needle (1D) and hierarchical cauliflower (3D) morphologies on galvanized steel substrates using a simple chemical bath deposition method. These nano/micro textured steel surfaces, on subsequent coating of a low surface energy material display excellent superhydrophobic, superoleophobic and slippery behavior. Polydimethylsiloxane coated textured surfaces illustrate superhydrophobicity with water contact angle about 160°(2) and critical sliding angle ~2°. When functionalized with low-surface energy perfluoroalkylsilane, these surfaces display high repellency for low surface tension oils as well as hydrocarbons. Among them, the hierarchical cauliflower morphology exhibits re-entrant structure thereby showing the best superoleophobicity with contact angle 149° for dodecane. Once infused with a lubricant like silicone oil, they show excellent slippery behavior with low contact angle hysteresis (~ 2°) for water drops.

Past decade has attracted tremendous scientific interest in superhydrophobic surfaces because of their potential applications in many fields, such as transport of microdroplets, biochemical separation, drug delivery, tissue engineering, anticorrosion, self-cleaning, drag-reduction coating and microfluidic lab-on-chip devices[1–12]. Inspired by the investigation on lotus leaf effect, synthetic superhydrophobic surfaces are fabricated on a variety of substrates including metals[13], glass[14], polymers[15] and fabrics[16] by combining hierarchical nano- and microstructures along with low surface energy fluorinated molecules, resulting in very high water contact angle (CA > 150°) and a very low sliding angle (SA < 10°)[17,18]. In addition to repelling water, superoleophobic surfaces repel organic liquids (oils/hydrocarbons) with low surface tensions and thus create surfaces which are resistant to organic contaminations[19]. However, in contrast to superhydrophobicity, achieving superoleophobicity entails a second essential feature related to a very specific surface morphology; i.e., re-entrant/overhanging surface features[19,20]. Generally, fabrication of surfaces with diminished wettability relies on roughness of textured surface since all non-textured (smooth) surfaces, regardless of their chemical compositions, are intrinsically oleophilic. Young's relation for determining wettability (contact angle θ_Y) of a liquid on smooth surface is given by:

$$\cos \theta_Y = (\gamma_{SV} - \gamma_{SL})/\gamma_{LV} \tag{1}$$

Department of Physics, Indian Institute of Technology Kanpur, Kanpur - 208016, India. Correspondence and requests for materials should be addressed to K.K. (email: kcharya@iitk.ac.in)

Here γ denotes the interfacial surface tension, and S, L, and V stands for solid, liquid and vapor phase, respectively. Non-textured surfaces, if modified with low surface energy fluorosilane molecules (one with lowest surface energy reported is $\gamma_{SV} = 6\,\text{mJ/m}^2$)[21] result in contact angle (θ_Y) < 90° for oils. For instance, hexadecane (surface tension $\gamma_{LV} = 27.6\,\text{mJ/m}^2$) showed $\theta_Y \sim 80°$ while for water (surface tension $\gamma_{LV} = 72.1\,\text{mJ/m}^2$) $\theta_Y \sim 120°$[22]. On surfaces with small roughness, contact angle is determined by Wenzel's relation as $\cos\theta^* = r\,\cos\theta_Y$ where r is the roughness parameter defined as the ratio of actual surface area to projected surface area[23]. In contrast, surfaces with large roughness modified with fluorinated silanes demonstrated $\theta > 150°$ for oils and $\theta > 160°$ for water[20] with very low roll-off angle ($\omega \leq 2°$) as the liquid droplets can be stabbed on the top of the roughness asperities due to pockets of air trapped underneath[24–36], as discussed by Cassie-Baxter relation:

$$\cos\theta^* = -1 + f(1 + \cos\theta_Y) \qquad (2)$$

where θ^* is defined as apparent contact angle on textured (rough) surface and f represents the area fraction of solid-liquid interface. Although this approach is promising, it suffers from inherent limitations related to irreversible defects arising during fabrication and mechanical damage which enhance pinning effect in the superhydrophobic surface and deteriorate liquid mobility[37]. In order to overcome these limitations, taking inspiration from Nepenthes pitcher plants[38], stable, defect-free and inert 'slippery' interface have been developed by lubricating liquid-infused porous surface in which micro, nanostructures locked the infused lubricant in place[37,39–48]. Lubricating fluid is intrinsically smooth and defect-free and can afford instantaneous self-repair by wicking into dent sites in the underlying substrate[37,38]. Lubricating fluid may not have the ability to self-repair in presence of ice as shown by Rykaczewski et al.[49]. Recently, Anand et al. has demonstrated reduced pinning of the condensate droplets by a hierarchical micro-nano textured surface by impregnating with an appropriate lubricant[50] while, Li et al. suggested self cleaning properties of hydrophobic liquid-infused porous poly(butyl methacrylate-co-ethylene dimethacrylate) surface[51].

Therefore, it would be worthwhile to notice that combination of the nano/micro, hierarchical and re-entrant structures along with well-matched solid and liquid surface energy is the most crucial parameter to create highly stable superhydrophobic, superoleophobic and slippery surfaces but making such robust textured roughness is challenging[37]. Although the current state-of-the-art have generated efficient surfaces with precise control of nano and micro structures, however reported fabrication processes for the creation of surface roughness involving lithographic means[37,52], micro-fabrication[53–55], self assembly[56,57], or by the use of polyelectrolyte multilayers (PEMs) assembled by the layer-by-layer technique[58], sol-gel methods[59], spin-coating[60], electrochemical deposition which requires a conductive substrate[61], and polymer imprinting[2,62–67] are sophisticated, costly and difficult to be implemented on a large scale. The complications are mostly associated with the manufacturing of a robust hierarchical structure with re-entrant and convex morphology which is the key for superoleophobicity.

Steel, considered to be the workhorse of our society as the most essential engineering material in field of construction, food, petrochemical, maritime and aviation industries[68]. Its broad applications can be further augmented by making it super-repellent for water/oil, especially for industries where metal−fluid contact is common. The super-repellency with such fluids provides resistance to fouling/corrosion properties which subsequently increases its life-time[69].

In this work, we have utilized relatively simple chemical bath deposition (CBD) technique for synthesizing four different morphologies of copper oxide (CuO) nano-/micro and hierarchical structures on steel substrates. The CBD method involves very simple instrumentation facility and can be used to fabricate a single crystalline material such as metal oxides and hydroxides on a wide variety of substrates, because in thermodynamic equilibrium conditions each metal complex in the precursor solution is singly deposited on the substrate surface[70]. Furthermore, these CuO nano-/micro textured steel substrates were coated with polymethylsiloxane (PDMS) by dip coating, resulting in highly robust superhydrophobic surfaces. The effect of micro-/nano structures on superhydrophobic, superoleophobic and lubricant based slippery behavior have been studied. Moreover, the fabrication conditions involved in the whole process are mild (low temperature, dilute solutions and air atmosphere) and fairly easy, required no sophisticated instrument.

Experimental Section

Materials.   Poly(dimethylsiloxane) (PDMS) pre-polymer (Sylgard 184A) and thermal curing agent (Sylgard 184B) were purchased from Dow Corning Corp. 1H,1H,2H,2H-perfluorooctyltriethoxy silane ($C_{14}H_{19}F_{13}O_3Si$) (PTES) was purchased from Alfa Aesar. Silicone oil ($\eta = 350\,\text{cSt}$), copper sulphate ($CuSO_4$), L-ascorbic acid, sodium hydroxide (NaOH) and sodium borohydride ($NaBH_4$) were of analytical grade and purchased from Loba Chemie. Sodium dodecyl sulphate (SDS), ethanol and toluene were procured from Merck. Galvanized steel (GI) substrates (Tata Steel, India) ($4\,\text{cm} \times 2\,\text{cm} \times 0.2\,\text{cm}$) were ultrasonically cleaned in acetone and then rinsed with de-ionized water sequentially before use.

Characterization.   The surface morphologies of the fabricated copper oxide particles on different substrates and the corresponding superhydrophobic PDMS films coated samples were investigated using field emission scanning electron microscopy (FESEM: JEOL, JXA-8230) at an accelerating voltage of 10 kV and RMS surface roughness was determined using atomic force microscope (AFM) (Park system XE-70) in a tapping mode in the range of scanning area of $3\,\mu\text{m} \times 3\,\mu\text{m}$. Powder X-ray diffraction (XRD) measurements of copper oxide nanoparticles grown on steel substrates were performed with a X'Pert Pro MPD X-Ray Diffractometer. Static contact angle (CA) (θ_S), Advancing contact angle (θ_A) and Receding contact angle (θ_R) were measured using Milli-Q water at room temperature with a Contact angle goniometer (OCA-35, DataPhysics, Germany). θ_S was measures using Laplace-Young fitting model of a $2\,\mu\text{l}$ water droplet placed on the horizontal glass substrate. θ_A and θ_R were measured by adding and then withdrawing $2\,\mu\text{l}$ of water drop respectively. The contact angle hysteresis ($\theta_A - \theta_R$)

(CAH) was obtained using the circle fitting method. Static tilt angle (α) was obtained by observing the minimum tilt angle required to move the water drop ($10\,\mu l$) from horizontal surface. The velocity of the drop ($10\,\mu l$) was measured by recording the movement of water drops on a tilted surface ($\alpha = 12°$) and then calculating the distance travelled per unit time. All θ and α value are in the range of $\pm 2°$. All the measurements were performed in duplicate on a given substrate and two such substrates for each composition. The values mentioned are average of these measurements.

Synthesis of copper oxide nanoparticles.

Morphology controlled growth of copper oxide nanoparticles film on Fe substrate in aqueous solvent was typically processed by bath deposition method. Equal volume of two aqueous sodium dodecyl sulfate (SDS) solutions (250 mg in 20 ml DI), one containing cupric sulphate ($CuSO_4.5H_2O$) (10 mM to 100 mM solution in DI water) and the other containing L-ascorbic acid (20 mM to 200 mM) were mixed by magnetic stirrer and temperature was kept constant at 70 °C. Color change occurred in the aqueous phase from blue to pale green and finally the solution turned colorless. The pH of the solution was adjusted to 11 using NaOH solution. On addition of NaOH solution, the colorless solution changed to yellow, reddish orange and reddish brown respectively, depending on the concentration of metal precursor solutions. The cleaned steel substrates of dimension (4 cm × 2 cm) were immersed in the above solution. After stirring for 10 min, 10 ml of (100 mM to 1M) $NaBH_4$ aqueous solution was drop wise added into the reaction vessel. On addition, all the solutions gradually became reddish black. The reaction mixture was further stirred overnight in ambient atmosphere at 70 °C, to allow the reaction to complete. Thin film of CuO nanoparticles formed on steel substrates was taken out and washed with ethanol and DI water to remove surfactant. The films were dried in air at 60 °C and used for further studies. For synthesizing CuO nanoparticles on PDMS film, glass and steel mesh substrates, highest precursor concentration (i.e. 100 mM $CuSO_4$) was used.

Preparation of PDMS coated superhydrophobic copper oxide textured steel.

Copper oxide nanoparticles textured steel surfaces were found to be superhydrophilic. In order to make them superhydrophobic, PDMS was used as a low surface energy material for the nanostructured substrates. PDMS pre-polymer and thermal curing agent (Sylgard®184, Dow Corning) were mixed in 2:1 ratio and diluted in 200 ml toluene. The nano-patterned surfaces were dip-coated in the solution (Apex Instrument, Model Xdip-SV1) with 200 mm/min lifting speed which were subsequently annealed at 110 °C for 30 min. Since it was not possible to measure the PDMS thickness on the nano-patterned substrates, a flat CuO surface was also used as control substrate and coated with PDMS using same parameters which gave PDMS thickness of 32 (± 6) nm as measured using an Atomic Force Microscope (AFM). Therefore we can assume that PDMS thickness on the nano-patterned substrates would also be in the range from 20–40 nm.

Surface modification by perfluoroalkylsilane.

The PDMS coated copper oxide textured steel samples were exposed to a UV Ozone cleaner for 10 min to oxidize the PDMS surface and generate oxygen functionalities[71]. These functionalities act as anchor sites for perfluoroalkylsilane grafting. In a typical process, the oxidized samples were placed in a vacuum chamber and $20\,\mu l$ of 1H,1H,2H,2H-perfluorooctyltriethoxysilane ($C_{14}H_{19}F_{13}O_3Si$) (PTES), deposited on a glass slide was placed at a sufficient minimum distance from samples. Under low pressure, PTES vapor was deposited on samples for 20 min.

Silicone oil infused slippery surface.

Slippery surfaces based on PDMS coated copper oxide textured steel surfaces infused with Silicone oil were prepared by immersing the steel samples in silicone oil for 2 min and then pulled out with a speed of 200 mm/min. The porous PDMS absorbs silicone oil and excess oil was removed by gravity drainage by hanging samples for 30 min. After gravity drainage, the substrates were spin coated at 500 rpm for 30 sec to provide uniformity in the oil film thickness. It is difficult to define the lubricating film thickness on nano-patterned substrates since most of the lubricant impregnates into the nano-pores formed by CuO nanostructures. For Set B samples, thickness of CuO nanostructure film is 5.44 (± 0.21) μm, therefore we expect that the thickness of the lubricating film on the nano-patterned substrates would be slightly more than the thickness of the nano-pattern itself. Along with the nano-patterned substrates, a control sample (flat CuO surface with thin PDMS layer) was also coated with silicone oil which resulted in oil film thickness of 4.3 (± 0.1) μm calculated by weight difference method. Based on these results, we expect the lubricating film thickness on the nano-patterned substrates in the range 5–6 μm.

Results and Discussion

Structure, morphology and roughness.

Morphology controlled synthesis of nano-crystals with well defined shape and uniform size has been achieved by several methods involving conventional solid state process and wet synthetic routes, such as hydrolysis, pyrolysis, precipitation, and hydrothermal/solvothermal. Among all these methods, the solution assisted synthesis by chemical bath deposition (CBD) of the precursor may be the most facile and effective approach to develop nano-crystals at relatively low temperatures, which is exempted from post calcination.

Besides this, CBD exhibits considerable influence of metal salt precursor ($CuSO_4$) concentration on the final structure and morphology of the as-prepared CuO patterns on steel substrate. All obtained CuO samples are of Base-centered monoclinic structure, space group: C2/c(15) (JCPDS Card No. 001-1117, a = 4.653 Å, b = 3.41 Å, c = 5.108 Å, b = 99.48°). The XRD pattern shown in Fig. 1 exhibits peak at 2θ : 35.74, 38.95, 53.88 corresponding to Miller indices (−111), (111) and (020), confirming CuO. Very diminished peak at 43.3° corresponds to (111) plane of Cu (JCPDS Card No. 01-070-3039). Presence of two characteristic peaks for Fe at 2θ: 44.65 and 64.98 corresponding to (110) and (200) Miller indices confirmed the presence of Fe substrate underneath CuO.

The summarized reaction conditions and morphologies are illustrated in Fig. 2 and the representative SEM and AFM images are shown in Fig. 3. The precursor solution for the crystallization of CuO was prepared using
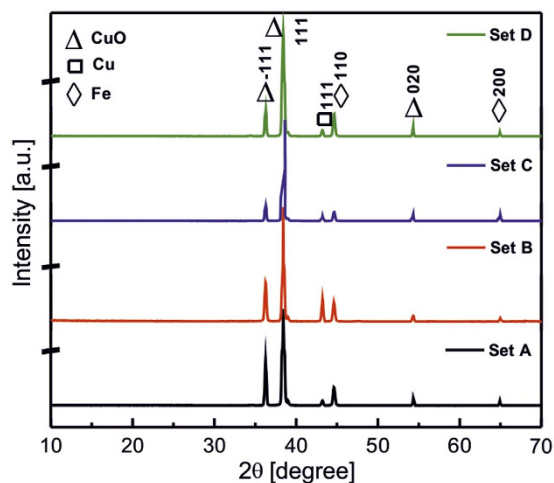
Figure 1. XRD pattern of CuO nanoparticles on steel substrates obtained by the chemical bath deposition method using different concentrations (Set A) 10 mM, (Set B) 20 mM, (Set C) 50 mM and (Set D) 100 mM aqueous CuSO$_4$ solution in the presence of the reducing agents ascorbic acid and sodium borohydride respectively at pH 11.
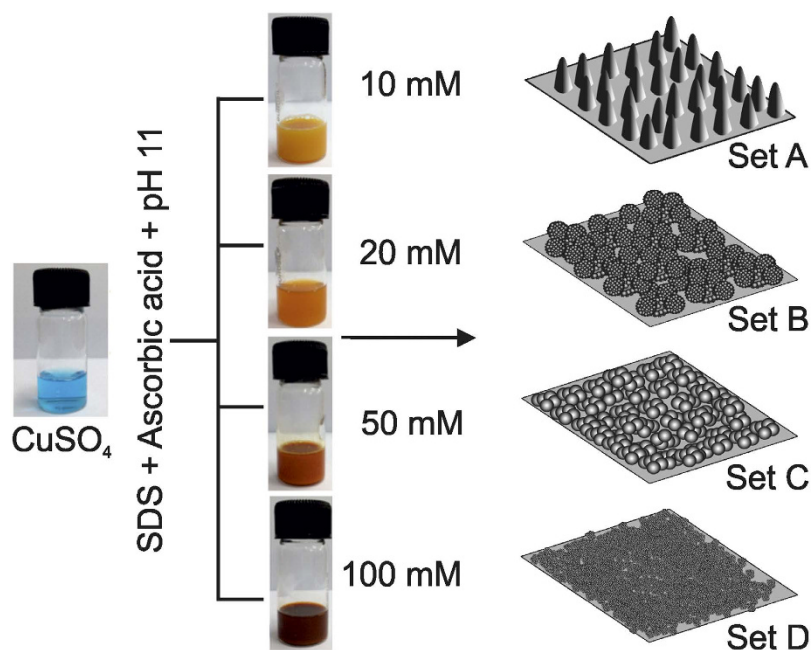

Figure 2. Schematic illustrating precursor concentration dependent CuO nano-/micro particles growth on steel substrates by chemical bath deposition method.

de-ionized water, CuSO$_4$, surfactant SDS, L-ascorbic acid, NaOH and NaBH$_4$ solution in the order depicted above. Depending on the concentration of aqueous SDS CuSO$_4$ solution (blue) from 10 to 100 mM, they demonstrate change in color from yellow to reddish wine on addition of L-ascorbic acid at constant pH 11. After adding reducing agent NaBH$_4$, the crystallization of CuO in different morphology took place. The increase in concentration of CuSO$_4$ induced a reduction in crystallite size probably due to enhancement of the nucleation rate which enhanced growth kinetics of nanocrystals. SEM images clearly demonstrate the delicate morphology control that can be achieved by adjusting the concentration of precursor solution. 10 mM CuSO$_4$ solution results in needle-like morphology with height around 1 μm, (Fig. 3a,e,i) which are almost perpendicular to the substrate. The images show that the needles are very sharp, with tip diameter in the range of tens of nanometer. Upon increasing the CuSO$_4$ concentration to 20 mM, hierarchical cauliflower like morphology is obtained with an average diameter of about 0.5 to 2 μm (Fig. 3b,f,j).

Figure 3 (c,g,k) display nano-sphere morphologies with an average diameter 80 nm obtained from 50 mM precursor solution. If concentration is further increased to 100 mM, the CuO nano-spheres get agglomerated resulting in larger clusters (Fig. 3d,h,l). Surface roughness of all the four morphologies calculated from the AFM images
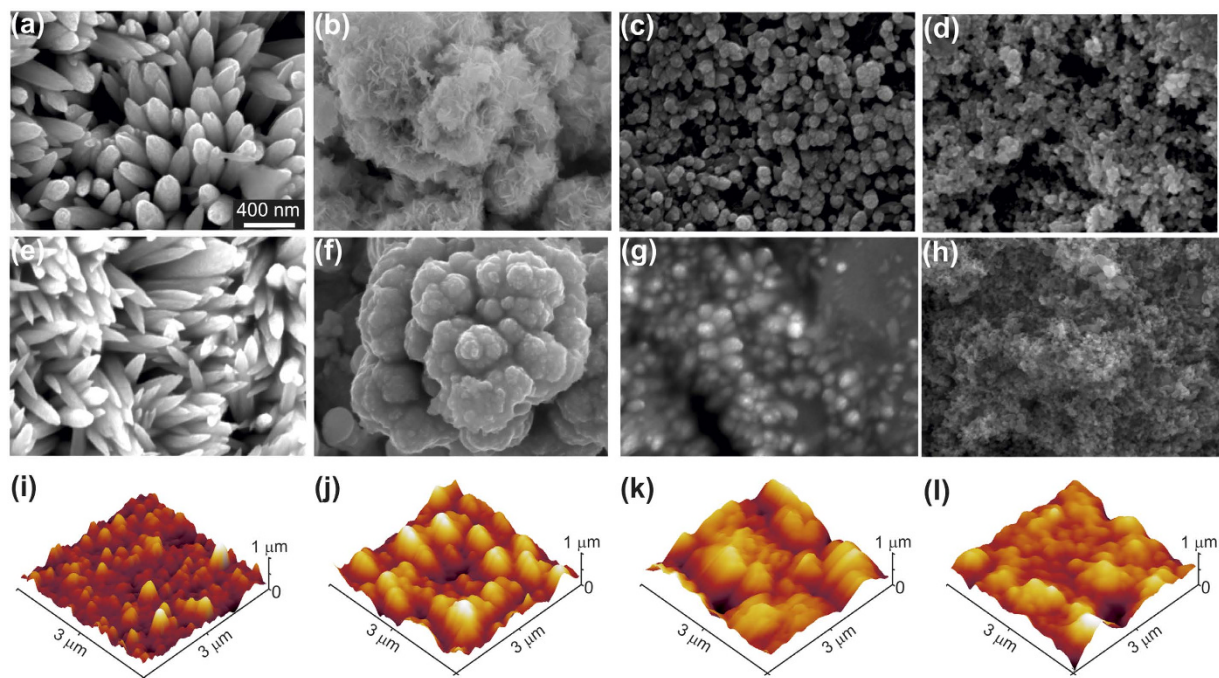
Figure 3. SEM and AFM images of CuO nanostructures obtained by CBD process by varying the concentration of CuSO$_4$ precursor solution. (**a**), (**e,i**) Nano-needle (10 mM), (**b**), (**f,j**) Hierarchical cauliflower (20 mM), (**c**), (**g,k**) nanosphere (50 mM) and (**d**), (**h,l**) nanosphere cluster (100 mM).

are 127.7 nm, 164.5 nm.143.7 nm and 132.9 nm for the nano-needle, hierarchical cauliflower, nanosphere and nanosphere cluster respectively. Thickness of the various CuO nanostructure coating was measured by mechanical profilometer and is shown in Supplementary Figure S1.

In order to reduce surface energy and improve mechanical stability, the hydrophilic CuO nano-patterns were dip coated in dilute PDMS solution followed by curing at 110 °C for 30 min. The resulting CuO nanopatterned surfaces shown in Fig. 3e–h, indicate no change in overall morphology. Here we should note nanoscale roughness in hierarchical cauliflower and nanosphere morphologies is smeared out due to PDMS filling, but we will later show that this does not affect any of the physical behavior of the system.

Mechanical stability of all the fabricated superhydrophobic samples were measured using tape test (ASTM D3359). A cross hatch cutter (Sheen Instruments, model SH750/3) was used to cut the coating followed by peeling with an adhesive tape and this cycle was repeated for 10 times. After each cycle, the surface morphology and wettability were observed to analyze the mechanical stability of the coating. The removed nanoparticles from the CuO nano-needle textured surface without PDMS coating and with PDMS coating were examined by SEM. Dense coverage of nano structures was found on the pealed tape from the surfaces without PDMS coating, while the coated surfaces didn't reveal much, indicating enhanced stability of nano patterns post PDMS coating. Subsequently, these PDMS coated CuO nano-textured steel surfaces with different morphologies and roughness were investigated for their wetting behavior under different conditions.

Superhydrophobicity. CuO nano-textured PDMS coated steel surface possesses large roughness due to presence of CuO of different morphologies and low surface energy due to PDMS, which is essential to achieve superhydrophobicity[20]. All four CuO nano-textured morphologies after PDMS coating exhibit prominent superhydrophobicity with water contact angles as high as 163° (Fig. 4a–d). The extreme water repellency of each surface also reflects very low contact angle hysteresis ($\Delta\theta \sim 2°$) and very low sliding angles ($\alpha \sim 2°$) for 2 μl droplet volume (Fig. 4e). The ultra-low contact angle hysteresis (difference between the advancing and receding contact angle of the droplet) and sliding angle (minimum surface tilt on which droplet starts moving) of these surfaces confirm uniformity and lack of pinning sites[37] which allowed water droplets to easily bounce and roll-off on them (Fig. 4f; see Supplementary Movie S1).

This superhydrophobic nature also protects the surfaces from wide range of contaminants by self-cleaning action which allows water droplets to collect and remove the contaminants from surfaces upon roll off (see Supplementary Movie S2). To demonstrate versatility of CBD based superhydrophobic coatings on variety of substrates, CuO nanopatterns were grown on glass, PDMS sheet and steel mesh followed by PDMS coating. Figure 5a–c shows electron microscope images of CuO nanoparticles based superhydrophobic samples on PDMS, glass and steel mesh along with optical micrographs and water drops. All these substrates showed excellent superhydrophobicity (water contact angle ~160°) and mechanical stability (see Supplementary Figure S2).

Superoleophobicity. To generate repellency towards low surface tension oils and hydrocarbons, the PDMS coated nano-textured surfaces were further functionalized with a low-surface energy perfluoroalkylsilane. Each
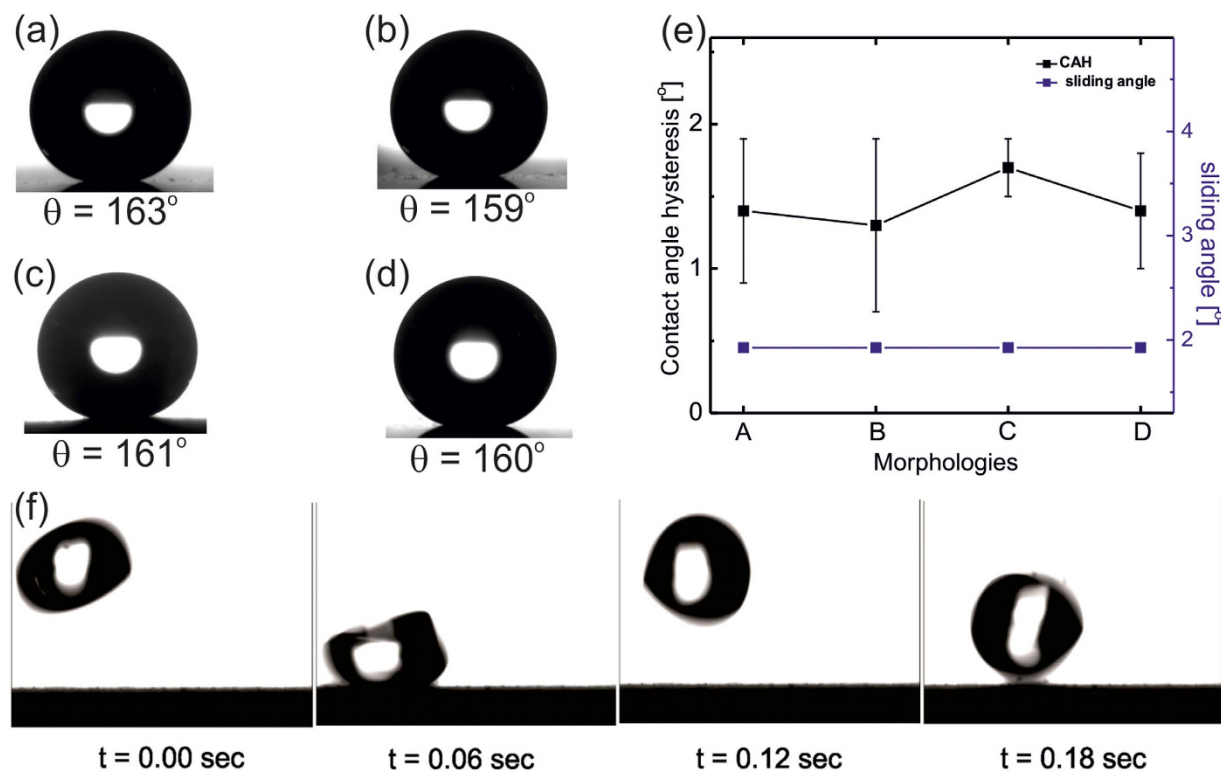
Figure 4. Water contact angle on samples with various morphologies: (**a**) nano-needle, (**b**) hierarchical cauliflower, (**c**) nanospheres and (**d**) nanosphere cluster, (**e**) Contact angle hysteresis and sliding angle plots for different morphologies, (**f**) water drop bouncing off a hierarchical cauliflower based superhydrophobic surface (Set B).
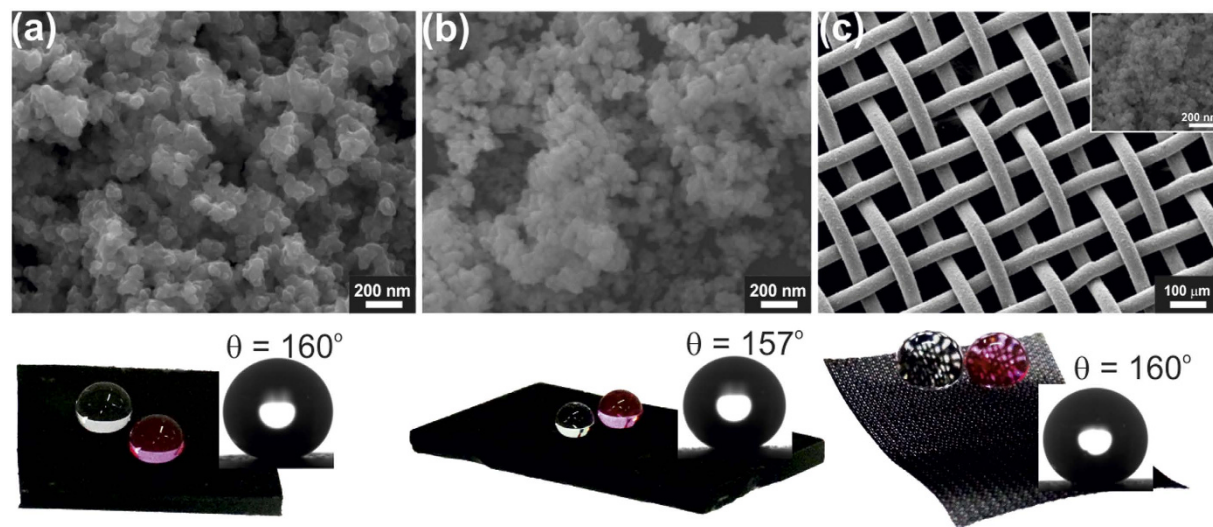

Figure 5. FESEM micrograph of CuO nanoparticles formed on (**a**) PDMS film, (**b**) glass and (**c**) steel mesh (Inset showing high magnification image). Their respective optical photograph with water droplets sitting on the surfaces and contact angle is also shown.

of these surfaces demonstrates extreme liquid repellency with contact angles 160° to 125° against liquids of surface tension ranging from 64.0 mNm^{-1} (glycerol) to 25.3 mNm^{-1} (dodecane) and depending on different morphologies (Fig. 6a).

The surface with cauliflower morphology having hierarchical nano-/micro structure with highest roughness displays higher contact angles, 160° for glycerol, which decreased to 149° for dodecane (Fig. 6(b,c); see Supplementary Movie S3 & Movie S4), while the nano-needle surface showed inferior repellency for low surface tension liquid, around 125° for dodecane. This is in agreement with previous reports discussing the ideal
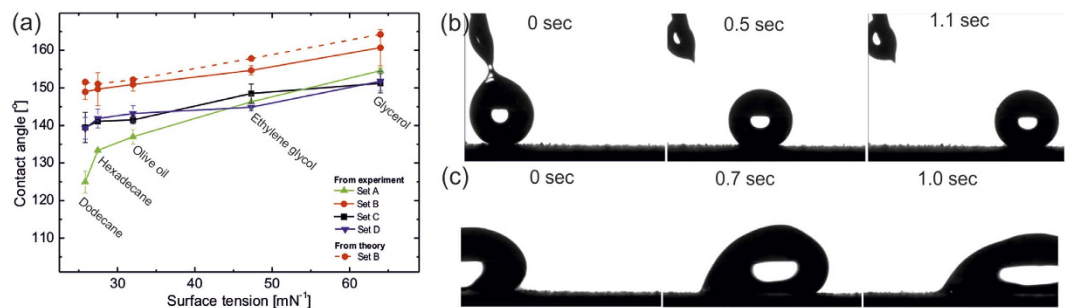
Figure 6. Superoleophobic behavior (**a**) Comparison of contact angle as a function of surface tension of test liquids on various morphologies of perfluoroalkylsilane functionalized PDMS coated CuO on steel substrates (Set A) nano-needle, (Set B) hierarchical cauliflower, (Set C) nanospheres and (Set D) nanosphere cluster. Corresponding theoretical value for Set B is shown with dotted line. Snaps of rolling glycerol (**b**) and dodacane (**c**) drops on hierarchical cauliflower (Set B) textured surface.

design parameters for superoleophobic surfaces having re-entrant geometry[20]. Hierarchically structured cauliflower surface, possessing re-entrant structure, can trap higher fraction of air at both the coarser and finer length scales showing extreme superoleophobicity while nano-needle structured surface has one scale of texture. Consequently, the former can support low surface tension liquids in the Cassie state resulting in superoleophobic surface. The substrates possessing a predominantly spherical textures (Set C and Set D) demonstrated intermediate superoleophobic behavior between the hierarchical and one scale textured.

As the cauliflower shape possesses re-entrant nanostructure and demonstrates the highest oleophobicity among the studied textures, we approximated the contact angles for different test liquids using equation (3)[19,20].

$$\cos \theta^*_{sphere} = -1 + \frac{1}{D^*_{sphere}}\left[\frac{\pi}{2\sqrt{3}}(1 + \cos \theta)\right]^2 \tag{3}$$

where, θ^* is the apparent contact angle on the textured surface and θ is the equilibrium contact angle on a smooth surface of the same substrate, given by Young's equation (1). D^* is the spacing ratio defining surface porosity and given by $D^*_{sphere} = \left[\frac{(R+D)}{R}\right]^2$ for spherical textured surface. Here, R defines the radius of the sphere and $2D$ is the inter-sphere distance. The theoretical values calculated using the above equation precisely matches the experimental data trend with highest contact angle 164° for glycerol and 151° for dodecane (Fig. 6a). The higher theoretical values for hierarchically textured surface are in agreement with the previous works on designing superoleophobic surfaces[20].

Silicone oil infused slippery surfaces (SOIS). SOIS were designed taking three criteria in consideration: (1) affinity of lubricating liquid with solid surface, i.e. the lubricating liquid must spread completely on the substrate, (2) slipping test liquid must be immiscible with the lubricant and (3) requirement of hydrophobic solid substrate. The first requirement is satisfied by using silicone oil, as it spreads completely on PDMS films. Since silicone oil is known to swell crosslinked PDMS, it is advantageous for our system as the swelling increases its adhesion with PDMS coated substrates. Second criterion was satisfied by taking water as a test liquid which shows immiscibility with silicone oil.

Third criterion is fulfilled automatically as PDMS coated substrates are inherently hydrophobic. Satisfying these criteria, we fabricated silicone oil infused nano textured slippery surfaces on steel substrates to slip water droplets upon tilting. Each of these SOIS demonstrates very low contact angle hysteresis ($\Delta\theta < 2°$) and low critical sliding angle ($\alpha < 2°$) and good slippery behavior with water drop velocity (≥ 1.05 mm/sec) for 10 μl droplet volume inclined at 12° (Fig. 7). Slippery behavior of the SOIS is found independent of underlying textured geometry provided sufficient lubricating fluid covers the entire surface. Static water drops deposited on silicone oil coated solid surfaces are cloaked with a thin layer of oil due to positive spreading coefficient of oil on water. Spreading parameter ($S_{OW(V)} = \gamma_{WV} - \gamma_{WO} - \gamma_{OV}$, subscript O, W and V represent oil, water and vapour respectively) for our system is 8.5 mN/m[72]. Once these oil cloaked water drops slip from the lubricant coated surface, they slowly remove oil from the surface thus decrease the lubricating layer thickness which affect the velocity of slipping water drop. We studied the effect of CuO nano morphology on the degradation of slippery behavior as a function of slipping water volume (Fig. 7a). It is clear from the figure that set B (hierarchical cauliflower) shows smallest degradation in slip velocity upon slipping water drops. This is due to the fact that the hierarchical cauliflower structures posses re-entrant geometry and lubricating oil trapped in the re-entrant structures are very hard to be removed. Therefore these structures show least degradation upon water flow compared to other structures. On the other hand, degradation on Set A sample is found to be the most due to their needle like structure. This degradation in slippery behavior of SOIS is related to the decreased lubricant thickness, which is also reflected in their increasing contact angle hysteresis (Fig. 7b). Expectedly, set B shows lowest increase in the contact angle hysteresis whereas set A shows the largest due to their underlying morphology. Self-healing ability of the SOIS is also checked by large area physical damage created on silicone oil film using a knife. Silicone oil lubricating film
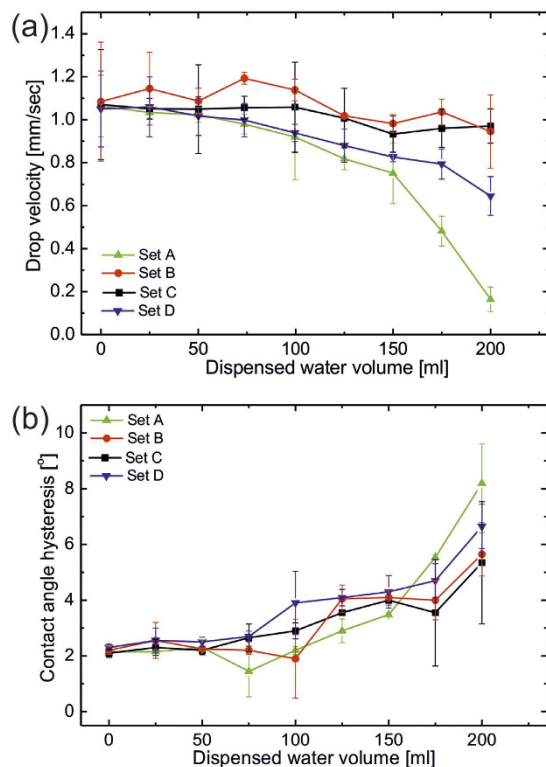
Figure 7. Silicone oil infused slippery behavior for water drops (**a**) Showing $10\,\mu l$ water drop velocity with volume of water dispensed and (**b**) contact angle hysteresis as a function of dispensed water volume of water dispensed over four different morphologies of Silicone oil infused PDMS coated CuO textured steel surfaces.

quickly heals the damage and restores the slippery behavior within fraction of seconds by filling the damaged void area by surface capillary action (see Supplementary Movie S5).

Conclusion

In this article, we have demonstrated a novel and convenient method to synthesize CuO nano-/micro structures with spherical (0D), needle (1D) and hierarchical (3D) cauliflower morphologies on steel substrate using chemical bath deposition (CBD). The change in morphology from 0D to 3D is precursor concentration dependent. Another advantage of this method is that, it is substrate independent and can be formed on polymer film, glass and mesh. On polydimethylsiloxane (PDMS) coating, these nano-/micro textured surfaces formed robust self-cleaning superhydrophobic surfaces with water drops bouncing on them as a consequence of low contact angle hysteresis ($\Delta\theta \leq 2°$) and sliding angle ($\alpha < 2°$). Perfluoroalkylsilane grafting resulted in low surface energy nano-/micro textured substrates showing repellency against various liquids with surface tension $\geq 25.3\,\mathrm{mNm}^{-1}$ (dodecane). The cauliflower morphology textured steel surface outperformed other morphologies in terms of different liquid repellency because of its hierarchical surface. In order to eliminate the constraints related to the self-healing on physical damage, silicone oil infused slippery surfaces (SOIS) were formed on these nano-/micro textured steel substrates. These SOIS demonstrated excellent slippery behavior for water with quick self-healing against physical damage. These results indicate that a suitable nano-/micro textured robust structures for desired application (superhydrophobic/superoleophobic/slippery) can be fabricated very easily on various substrates. We expect this low-cost, fast and convenient method will pave a new way for designing and fabricating robust textured surfaces for numerous applications in research and industrial field.

References

1. Choi, C.-H. & Kim, C.-J. Large slip of aqueous liquid flow over a nanoengineered superhydrophobic surface. *Phys. Rev. Lett.* **96,** 066001 (2006).
2. Lafuma, A. & Quere, D. Superhydrophobic states. *Nat. Mater.* **2,** 457–460 (2003).
3. Liu, H., Szunerits, S., Xu, W. & Boukherroub, R. Preparation of superhydrophobic coatings on zinc as effective corrosion barriers. *ACS Appl. Mater. Interfaces* **1,** 1150–1153 (2009).
4. Liu, T. *et al.* Corrosion behavior of super-hydrophobic surface on copper in seawater. *Electrochim. Acta* **52,** 8003–8007 (2007).
5. Liu, X., Liang, Y., Zhou, F. & Liu, W. Extreme wettability and tunable adhesion: Biomimicking beyond nature? *Soft Matter* **8,** 2070–2086 (2012).
6. Ou, J. & Rothstein, J. P. Direct velocity measurements of the flow past drag-reducing ultrahydrophobic surfaces. *Phys. Fluids* **17,** 103606 (2005).
7. Shirtcliffe, N. J., McHale, G., Newton, M. I. & Zhang, Y. Superhydrophobic copper tubes with possible flow enhancement and drag reduction. *ACS Appl. Mater. Interfaces* **1,** 1316–1323 (2009).
8. Yong, J. *et al.* Controllable adhesive superhydrophobic surfaces based on PDMS microwell arrays. *Langmuir* **29,** 3274–3279 (2013).

9. Hao, C. *et al.* Bioinspired Interfacial Materials with Enhanced Drop Mobility: From Fundamentals to Multifunctional Applications. *Small* **12,** 1825–1839 (2016).

10. Schellenberger, F. *et al.* Direct observation of drops on slippery lubricant-infused surfaces. *Soft Matter* **11,** 7617–7626 (2015).

11. Yohe, S. T., Colson, Y. L. & Grinstaff, M. W. Superhydrophobic materials for tunable drug release: using displacement of air to control delivery rates. *J. Am. Chem. Soc.* **134,** 2016–2019 (2015).

12. Salgado, C. L., Oliveira, M. B. & Mano, J. F. Combinatorial cell–3D biomaterials cytocompatibility screening for tissue engineering using bioinspired superhydrophobic substrates. *Integr. Biol.* **4,** 318–327 (2012).

13. Liu, K. & Jiang, L. Metallic surfaces with special wettability. *Nanoscale* **3,** 825–838 (2011).

14. Nakajima, A., Fujishima, A., Hashimoto, K. & Watanabe, T. Preparation of Transparent Superhydrophobic Boehmite and Silica Films by Sublimation of Aluminum Acetylacetonate. *Adv. Mater.* **11,** 1365–1368 (1999).

15. Shiu, J. Y., Kuo, C. W., Chen, P. & Mou, C. Y. Fabrication of Tunable Superhydrophobic Surfaces by Nanosphere Lithography. *Chem. Mater.* **16,** 561–564 (2004).

16. Ma, M., Mao, Y., Gupta, M., Gleason, K. K. & Rutledge, G. C. Superhydrophobic fabrics produced by electrospinning and chemical vapor deposition. *Macromolecules* **38,** 9742–9748 (2005).

17. Li, X.-M., Reinhoudt, D. & Crego-Calama, M. What do we need for a superhydrophobic surface? A review on the recent progress in the preparation of superhydrophobic surfaces. *Chem. Soc. Rev.* **36,** 1350–1368 (2007).

18. Sun, T., Feng, L., Gao, X. & Jiang, L. Bioinspired surfaces with special wettability. *Acc. Chem. Res.* **38,** 644–652 (2005).

19. Tuteja, A. *et al.* Designing superoleophobic surfaces. *Science* **318,** 1618–1622 (2007).

20. Kota, A. K., Mabry, J. M. & Tuteja, A. Superoleophobic surfaces: design criteria and recent studies. *Surface Innovations* **1,** 71–83 (2013).

21. Adamson, A. W. & Gast, A. P. *Physical Chemistry of Surfaces.* 368 (John Wiley & Sons, 1997).

22. Mittal, K. L. *Contact angle, Wettability and Adhesion* Vol. 5 (VSP Intl Science: Leiden, 2008).

23. Wenzel, R. N. Resistance of solid surfaces to wetting by water. *Ind. Eng. Chem.* **28,** 988–994 (1936).

24. Li, T. *et al.* Facile One-Step Photolithographic Method for Engineering Hierarchically Nano/Microstructured Transparent Superamphiphobic Surfaces. *ACS Appl. Mater. Interfaces* **7,** 10988–10992 (2015).

25. Cassie, A. B. D. Contact angles. *Discuss. Faraday Soc.* **3,** 11–16 (1948).

26. Bico, J., Marzolin, C. & Quere, D. Pearl drops. *Europhys. Lett.* **47,** 743–744 (1999).

27. Herminghaus, S. Roughness-induced non-wetting. *Europhys. Lett.* **52,** 165–170 (2000).

28. Joseph, P. *et al.* Slippage of Water Past Superhydrophobic Carbon Nanotube Forests in Microchannels. *Phys. Rev. Lett.* **97,** 156104 (2006).

29. Liu, Y. *et al.* Pancake bouncing on superhydrophobic surfaces. *Nat. Phys.* **10,** 515–519 (2014).

30. Tesler, A. B. *et al.* Extremely durable biofouling-resistant metallic surfaces based on electrodeposited nanoporous tungstite films on steel. *Nat. Commun.* **6,** 8649 (2015).

31. Schellenberger, F., Encinas, N., Vollmer, D. & Butt, H.-J. How Water Advances on Superhydrophobic Surfaces. *Phys. Rev. Lett.* **116,** 096101 (2016).

32. Schaffel, D., Koynov, K., Vollmer, D. & Butt, H.-J. & Schonecker, C. Local Flow Field and Slip Length of Superhydrophobic Surfaces. *Phys. Rev. Lett.* **116,** 134501 (2016).

33. Lu, Y. *et al.* Creating superhydrophobic mild steel surfaces for water proofing and oil–water separation. *J. Mater. Chem. A* **2,** 11628–11634 (2014).

34. Chen, X. *et al.* Fabrication of Functionalized Copper Compound Hierarchical Structure with Bionic Superhydrophobic Properties. *J. Phys. Chem. C* **113,** 5396–5401 (2009).

35. Patankar, N. A. Mimicking the lotus effect: Influence of double roughness structures and slender pillars. *Langmuir* **20,** 8209–8213 (2004).

36. Miwa, M., Nakajima, A., Fujishima, A., Hashimoto, K. & Watanabe, T. Effects of the surface roughness on sliding angles of water droplets on superhydrophobic surfaces. *Langmuir* **16,** 5754–5760 (2000).

37. Wong, T.-S. *et al.* Bioinspired self-repairing slippery surfaces with pressure-stable omniphobicity. *Nature* **477,** 443–447 (2011).

38. Bohn, H. F. & Federle, W. Insect aquaplaning: Nepenthes pitcher plants capture prey with the peristome, a fully wettable water-lubricated anisotropic surface. *Proc. Natl. Acad. Sci. USA* **101,** 14138–14143 (2004).

39. Kim, P., Kreder, M. J., Alvarenga, J. & Aizenberg, J. Hierarchical or not? Effect of the length scale and hierarchy of the surface roughness on omniphobicity of lubricant-infused substrates. *Nano Lett.* **13,** 1793–1799 (2013).

40. Leslie, D. C. *et al.* A bioinspired omniphobic surface coating on medical devices prevents thrombosis and biofouling. *Nat. Biotechnol.* **32,** 1134–1140 (2014).

41. Shillingford, C., MacCallum, N., Wong, T.-S., Kim, P. & Aizenberg, J. Fabrics coated with lubricated nanostructures display robust omniphobicity. *Nanotechnology* **25,** 014019 (2014).

42. Sunny, S., Vogel, N., Howell, C., Vu, T. L. & Aizenberg, J. Lubricant-Infused Nanoparticulate Coatings Assembled by Layer-by-Layer Deposition. *Adv. Func. Mater.* **24,** 6658–6667 (2014).

43. Anand, S., Rykaczewski, K., Subramanyam, S. B., Beysens, D. & Varanasi, K. K. How droplets nucleate and grow on liquids and liquid impregnated surfaces. *Soft Matter* **11,** 69–80 (2015).

44. Hao, C. *et al.* Superhydrophobic-like tunable droplet bouncing on slippery liquid interfaces. *Nat. Commun.* **6,** 7986 (2015).

45. Howell, C. *et al.* Stability of Surface-Immobilized Lubricant Interfaces under Flow. *Chem. Mater.* **27,** 1792–1800 (2015).

46. Sun, X., Damle, V. G., Liu, S. & Rykaczewski, K. Bioinspired Stimuli-Responsive and Antifreeze-Secreting Anti-Icing Coatings. *Adv. Mater. Interfaces* **2,** 1400479 (2015).

47. Wexler, J. S., Jacobi, I. & Stone, H. A. Shear-Driven Failure of Liquid-Infused Surfaces. *Phys. Rev. Lett.* **114,** 168301 (2015).

48. Golovin, K. *et al.* Designing durable icephobic surfaces. *Sci. Adv.* **2,** 1501496 (2016).

49. Rykaczewski, K. S. A., Subramanyam, S. B. & Varanasi, K. K. Mechanism of Frost Formation on Lubricant-Impregnated Surfaces. *Langmuir* **29,** 5230–5238 (2013).

50. Anand, S., Paxson, A. T., Dhiman, R., Smith, J. D. & Varanasi, K. K. Enhanced Condensation on Lubricant-Impregnated Nanotextured Surfaces. *ACS Nano* **6,** 10122–10129 (2012).

51. Li, J. *et al.* Hydrophobic Liquid-Infused Porous Polymer Surfaces for Antibacterial Applications. *ACS Appl. Mater. Interfaces* **5,** 6704–6711 (2013).

52. Smith, J. D. *et al.* Droplet mobility on lubricant-impregnated surfaces. *Soft Matter* **9,** 1772–1780 (2013).

53. Kramer, N., Birk, H., Jorritsma, J. & Schonenberger, C. Fabrication of metallic nanowires with a scanning tunneling microscope. *Appl. Phys. Lett.* **66,** 1325 (1995).

54. Murray Gibson, J. Reading and writing with electron beams. *Phys. Today* **50,** 56–61 (1997).

55. Oner, D. & McCarthy, T. J. Ultrahydrophobic Surfaces. Effects of Topography Length Scales on Wettability. *Langmuir* **16,** 7777–7782 (2000).

56. Genzer, J. & Efimenko, K. Creating long-lived superhydrophobic polymer surfaces through mechanically assembled monolayers. *Science* **290,** 2130–2133 (2000).

57. Zhai, L., Cebeci, F. C., Cohen, R. E. & Rubner, M. F. Stable Superhydrophobic Coatings from Polyelectrolyte Multilayers. *Nano Lett.* **4,** 1349–1353 (2004).

58. Huang, X., Chrisman, J. D. & Zacharia, N. S. Omniphobic Slippery Coatings Based on Lubricant-Infused Porous Polyelectrolyte Multilayers. *ACS Macro Lett.* **2,** 826–829 (2013).
59. van der Wal, P. & Steiner, U. Super-hydrophobic surfaces made from Teflon. *Soft Matter* **3,** 426–429 (2007).
60. Erbil, H. Y., Demirel, A. L., Avci, Y. & Mert, O. Transformation of a simple plastic into a superhydrophobic surface. *Science* **299,** 1377–1380 (2003).
61. Kim, P. *et al.* Liquid-Infused Nanostructured Surfaces with Extreme Anti-Ice and Anti-Frost Performance. *ACS Nano* **6,** 6569–6577 (2012).
62. Feng, X. J. & Jiang, L. Design and Creation of Superwetting/Antiwetting Surfaces. *Adv. Mater.* **18,** 3063–3078 (2006).
63. Guo, C. *et al.* Large-Area Fabrication of a Nanostructure-Induced Hydrophobic Surface from a Hydrophilic Polymer. *ChemPhysChem* **5,** 750–753 (2004).
64. Guo, Z., Zhou, F., Hao, J. & Liu, W. Stable Biomimetic Super-Hydrophobic Engineering Materials. *J. Am. Chem. Soc.* **127,** 15670–15671 (2005).
65. Lee, Y., Park, S. H., Kim, K. B. & Lee, J. K. Fabrication of Hierarchical Structures on a Polymer Surface to Mimic Natural Superhydrophobic Surfaces. *Adv. Mater.* **19,** 2330–2335 (2007).
66. Qian, B. & Shen, Z. Fabrication of Superhydrophobic Surfaces by Dislocation-Selective Chemical Etching on Aluminum, Copper, and Zinc Substrates. *Langmuir* **21,** 9007–9009 (2005).
67. Zhao, N. *et al.* A Lotus-Leaf-Like Superhydrophobic Surface Prepared by Solvent-Induced Crystallization. *ChemPhysChem* **7,** 824–827 (2006).
68. Cobb, H. M. *The History of Stainless Steel.* (ASM International, 2010).
69. Li, L., Breedveld, V. & Hess, D. W. Creation of Superhydrophobic Stainless Steel Surfaces by Acid Treatments and Hydrophobic Film Deposition. *ACS Appl. Mater. Interfaces* **4,** 4549–4556 (2012).
70. Hosono, E., Fujihara, S., Honma, I. & Zhou, H. Superhydrophobic Perpendicular Nanopin Film by the Bottom-Up Process. *J. Am. Chem. Soc.* **127,** 13458–13459 (2005).
71. Khare, K., Zhou, J. & Yang, S. Tunable Open-Channel Microfluidics on Soft Poly(dimethylsiloxane) (PDMS) Substrates with Sinusoidal Grooves. *Langmuir* **25,** 12794–12799 (2009).
72. Pant, R., Roy, P. K., Nagarajan, A. K. & Khare, K. Slipperiness and stability of hydrophilic surfaces coated with a lubricating fluid. *RSC Adv.* **6,** 15002–15007 (2016).

Acknowledgements

Author Contributions

S.K.U. and P.K.R. contributed equally to this work. Conceived and designed the experiments: S.K.U., P.K.R. and K.K. Performed the experiments: S.K.U., P.K.R., S.K. and S.S. Analyzed the data: S.K.U., K.K. and P.K.R. Contributed reagents/materials/analysis tools: K.K. Wrote the paper: S.K.U. and K.K.

Additional Information

Supplementary information accompanies this paper at http://www.nature.com/srep

Competing financial interests: The authors declare no competing financial interests.

How to cite this article: Ujjain, S. K. *et al.* Uniting Superhydrophobic, Superoleophobic and Lubricant Infused Slippery Behavior on Copper Oxide Nano-structured Substrates. *Sci. Rep.* **6**, 35524; doi: 10.1038/srep35524 (2016).